Journal of Photochemistry and Photobiology A: Chemistry 256 (2013) 52–63

Contents lists available at SciVerse ScienceDirect

Journal of Photochemistry and Photobiology A: Chemistry

journal homepage: www.elsevier.com/locate/jphotochem

TiON and TiON-Ag sputtered surfaces leading to bacterial inactivation under indoor actinic light

Sami Rtimi [a,d], Oualid Baghriche [a], Rosendo Sanjines [b], Cesar Pulgarin [a,**], Michael Bensimon [c], John Kiwi [e,*]

[a] Ecole Polytechnique Fédérale de Lausanne, EPFL-SB-ISIC-GPAO, Station 6, CH-1015 Lausanne, Switzerland
[b] Ecole Polytechnique Fédérale de Lausanne, EPFL-SB-IPMC-LNNME, Bat PH, Station 3, CH-1015 Lausanne, Switzerland
[c] Ecole Polytechnique Fédérale de Lausanne, EPFL-ENAC-IIEGR-CEL, Bat GC, Station 18, CH-1015 Lausanne, Switzerland
[d] UR Catalyse et Matériaux pour l'Environnement et les Procédés (URCMEP), Faculté des Sciences de Gabès, Université de Gabès, Gabès 6072, Tunisia
[e] Ecole Polytechnique Fédérale de Lausanne, EPFL-SB-ISIC-LPI, Bat Chimie, Station 6, CH-1015 Lausanne, Switzerland

ARTICLE INFO

Article history:
Received 31 October 2012
Received in revised form 4 February 2013
Accepted 9 February 2013
Available online 18 February 2013

Keywords:
DC-sputtering
TiON films
TiON-Ag films
Interfacial charge transfer
E. coli

ABSTRACT

This study reports the details *Escherichia coli* inactivation kinetics on TiON and TiON-Ag films sputtered on polyester by direct current reactive magnetron sputtering (DC) and pulsed magnetron sputtering (DCP) in an $Ar/N_2/O_2$ atmosphere. The use of TiON leads to bacterial inactivation avoiding leaching of Ag. The surface of TiON and TiON-Ag was characterized by X-ray photoelectron spectroscopy (XPS), atomic force microscopy (AFM), electron microscopy (EM), X-ray fluorescence (XRF) and contact angle (CA) measurements. Evidence for the photocatalyst self-cleaning after the bacterial inactivation was shown by XPS, contact angle (CA) and the Zetasizer zeta-potential of the proteins. The photo-induced charge transfer from Ag_2O and TiO_2 is discussed considering the relative positions of the electronic bands of the two oxides. An interfacial charge transfer mechanism (IFCT) for the photo-induced electron injection is suggested. The most suitable TiON coating sputtered on polyester was 70 nm thick and inactivated *E. coli* within 120 min under low intensity visible/actinic light (400–700 nm, 4 mW/cm^2). TiON-Ag sputtered catalysts shortened *E. coli* inactivation to ~55 min, since Ag accelerated bacterial inactivation due to its disinfecting properties. Evidence is presented for the repetitive performance within short times of the TiON and TiON-Ag polyester under low intensity visible light.

1. Introduction

Antimicrobial nanoparticulate films preparation is a topic of increasing attention since their objective is to reduce or eliminate the formation of infectious bacteria biofilms leading to hospital acquired infections (HAIs) [1–4]. Films presenting a more effective bacterial inactivation are needed due to the increasing resistance of pathogenic bacteria to synthetic antibiotics administered for long times [5]. Recently, Mills [6], Parkin [7–10], Foster [11], Dunlop [12] and Yates [13] have reported antibacterial Ag, Cu, and TiO_2 coatings on glass and polymer films depositing the metal/oxides by CVD and sputtering techniques. Chemical vapor deposition (CVD) is a chemical process used to produce high-purity, high-performance solid materials. In a typical CVD process, the wafer (substrate) is exposed to one or more volatile precursors, which react and/or decompose on the substrate surface to produce the desired deposit. Microfabrication processes widely use CVD to deposit materials in various forms, including: monocrystalline, polycrystalline, amorphous, and epitaxial.

Our laboratory has reported recently the antibacterial properties and kinetics of Ag- and Cu-modified textiles deposited by DC-magnetron, pulsed DC-magnetron and high power impulse magnetron sputtering (HIPIMS) [14–18].

Kelly has reported TiN and other nitrides co-sputtered with Ag able to inactivate Gram-negative and Gram-positive bacteria in the dark [19,20]. Reporting the important observation that Ag was immiscible with TiN. In this work we present the bactericide activity of TiON and TiON-Ag sputtered films under visible light irradiation. Ag is a non-cytotoxic bactericide agent at low concentrations [21]. But when washing Ag sputtered textiles, Ag leaches out of the textile surface and becomes an undesired environmental problem [22]. The exposure data of Ag furtive leaching and their possible toxicity is still lacking [23]. *E. coli* inactivation of TiON layers under visible light avoids the environmental Ag-leaching of Ag-based disinfecting materials.

There has been recently an interest in the preparation of TiON-films with intermediate behavior between metallic TiN and insulating TiO_2. These films are used in interconnectors in the

* Corresponding author. Tel.: +41 215348261; fax: +41 216935690.
** Corresponding author. Tel.: +41 216934720; fax: +41 216935690.
E-mail addresses: cesar.pulgarin@epfl.ch (C. Pulgarin), john.kiwi@epfl.ch (J. Kiwi).

1010-6030/$ – see front matter © 2013 Elsevier B.V. All rights reserved.
http://dx.doi.org/10.1016/j.jphotochem.2013.02.005

electrical industry [24]. Thin nitrides films present high chemical resistance to corrosion/oxidation, high melting point and acceptable adhesion [25]. Nitrides are at present explored for biomedical applications like implants due to its biocompatibility and long-term corrosion resistance [26]. N-doped titanium oxide films have been reported to improve the visible absorption range of TiO_2 since N-atoms occupy the O-atom sites in the TiO_2 lattice forming Ti—O—N bonds, red shifting the TiO_2 light absorption [27,28].

The objectives of this study are: (a) to optimize the film composition and light intensity on the TON-Ag films to attain the shortest inactivation time for *E. coli*, (b) to test the stability of TiON-Ag and TiON samples during *E. coli* inactivation, (c) to suggest an interfacial charge transfer mechanism (IFCT for the photo-induced electron transfer from Ag_2O to TiO_2 and finally, and (d) to characterize the TiON-Ag by surface science techniques allowing to describe the structure of this film.

2. Experimental

2.1. Sputtering of TiON and TiON-Ag on polyester

The TiON was DC-sputtered on polyester. The composite TiON-Ag was sputtered by DCP. The sputtering details have been previously reported out of our laboratory [29–31]. Before sputtering the films, the residual pressure P_r in the sputtering chamber was $P_r \leq 10^{-4}$ Pa. The substrate target distance was varied between 8.5 and 11 cm but for most of the runs the distance was kept at ~11 cm. The TiON thin films were deposited by reactive DC-magnetron sputtering (DC) in an $Ar + N_2 + O_2$ gas flow from a 5 cm diameter Ti-target 99.99% pure (Kurt J. Lesker, East Sussex, UK). The sputtering current on the Ti target was set at 280 mA, at a power of 128 W (U-518 V). DCP was used to sputter Ag and was operated at 50 kHz with 15% reversed voltage. The sputtering current was set at 280 mA with U-500 V, 75 V reverse voltage (15% of 500 V) and a power of 140 W.

The substrate used for the sputtered films was polyester (PET) presenting excellent durability during long-term operation, good abrasion resistance, fiber appearance retention, elasticity, stress recovery and resiliency. The polyester used corresponds to the EMPA test cloth sample No 407. It is a polyester Dacron polyethylene-terephthalate, type 54 spun, plain weave ISO 105-F04 used for color fastness determinations. The thermal stability of Dacron polyethylene terephthalate was 115 °C for long-range operation and 140 °C for times ≤1 min. The thickness of the polyester was ~130 μm. The polyester samples were 2 cm × 2 cm in size.

2.2. X-ray fluorescence determination of the Ag and Ti on polyester samples (XRF)

The Ag-content on the polyester was evaluated by X-ray fluorescence (XRF) in a PANalytical PW2400 spectrometer. Each element emits an X-ray of a certain wavelength associated with its particular atomic number.

2.3. Evaluation of the bacterial inactivation of E. coli on polyester under light irradiation

The samples of *Escherichia coli* (*E. coli* K12) was obtained from the Deutsche Sammlung von Mikroorganismen und Zellkulturen GmbH (DSMZ) ATCC23716, Braunschweig, Germany, to test the antibacterial activity of the Ag-polyester sputtered fabrics. The polyester fabrics were sterilized by autoclaving at 121 °C for 2 h. The 20 μL culture aliquots with an initial concentration of ~10^6 CFU mL^{-1} in NaCl/KCl (pH 7) were placed on coated and uncoated (control) polyester fabric. The polyester is a microporous substrate and distributes the inoculum evenly on the TiON, TiON-Ag films without needing an adsorption stage. A well-dispersed non-heterogeneous contact is established between the sample and the bacterial solution. The 20-μL of the *E. coli* solution was contacted with the TiON and TiON-Ag uniform films. The distribution of bacteria on the sputtered polyester was observed to be perfectly homogeneous and kill the inoculated cells on contact. The exposition was done at 25–28 °C. The samples were then placed on Petri dishes provided with a lid to prevent evaporation. After each determination, the fabric was transferred into a sterile 2 mL Eppendorf tube containing 1 mL autoclaved NaCl/KCl saline solution. This solution was subsequently mixed thoroughly using a Vortex for 3 min. Serial dilutions were made in NaCl/KCl solution. A 100 μL sample of each dilution was pipetted onto a nutrient agar plate and then spread over the surface of the plate using standard plate method. Agar plates were incubated lid down, at 37 °C for 24 h before colonies were counted. Three independent assays were done for each sputtered sample.

The statistical analysis of the results was performed for the CFU values calculating the standard deviation values. The average values were compared by one-way analysis of variance and with the value of statistical significance. The one-way analysis of variance (one-way ANOVA) was used to compare the mean of the samples using the Fisher distribution. The response variable was approximated for the sample data obtained from the photocatalytic inactivation of test samples presenting the same distribution within the same sputtering time.

To verify that no re-growth of *E. coli* occurs after the first bacterial inactivation cycle, the TiON-Ag nanoparticle film was incubated for 24 h at 37 °C. Then, the bacterial suspension of 100 μL is deposited on three Petri dishes to obtain the replica samples of the bacterial counting. These samples were incubated at 37 °C for 24 h. No bacterial re-growth was observed.

The irradiation of the polyester samples was carried out in a cavity provided with tubular Osram Lumilux 18 W/827 actinic lamp. These lamps emitted in the visible between 400 and 700 nm with an integral output of 1.0 mW/cm^2 resembling the light distribution found in solar irradiation. These lamps are used in hospital indoor illumination presenting an efficient compromise of energy consumption and the intensity of the emitted light.

2.4. Diffuse reflectance spectroscopy (DRS)

Diffuse reflectance spectroscopy was carried out a Perkin Elmer Lambda 900 UV–vis–NIR spectrometer provided for with a PELA-1000 accessory within the wavelength range of 200–800 nm and a resolution of one nm. The absorption of the samples was plotted in Fig. 9 in the Kubelka–Munk (KM) unit's vs. wavelength.

2.5. Transmission electron microscopy (TEM) and energy dispersive spectroscopy (EDS)

A Philips CM-12 (field emission gun, 300 kV, 0.17 nm resolution) microscope at 120 kV was used to measure grain size of the Ag-films. The textiles were embedded in epoxy resin 45359 Fluka and the fabrics were cross-sectioned with an ultramicrotome (Ultracut E) at a knife angle at 35°. Images were taken in bright-field (BF) mode for the samples of TiON-Ag (4 min–30 s). EDX was used to determine the chemical surface composition at the current beam position. Atoms of different chemical elements emit X-rays with a different specific energy.

2.6. Atomic force microscopy (AFM) and contact angle (CA) determination

Measurements were performed with a Parks Scientific XE120 AFM in contact mode. The Cantilever used was an Olympus

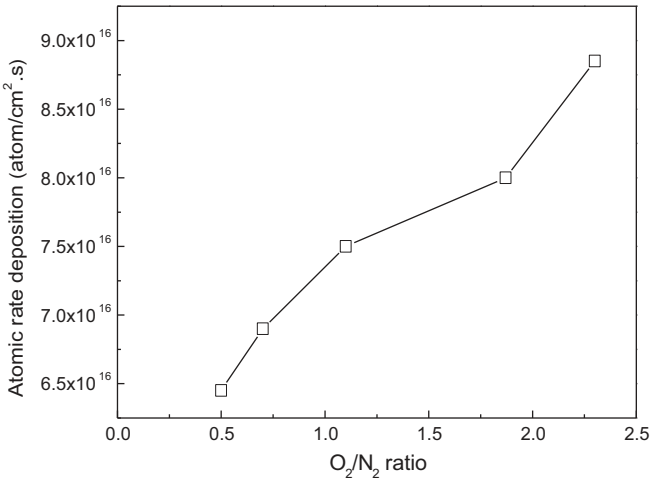

Fig. 1. Atomic deposition rate of TiON films on polyester as a function of the O_2/N_2 ratio. Ar gas flow was 90% at a working pressure 0.5 Pa.

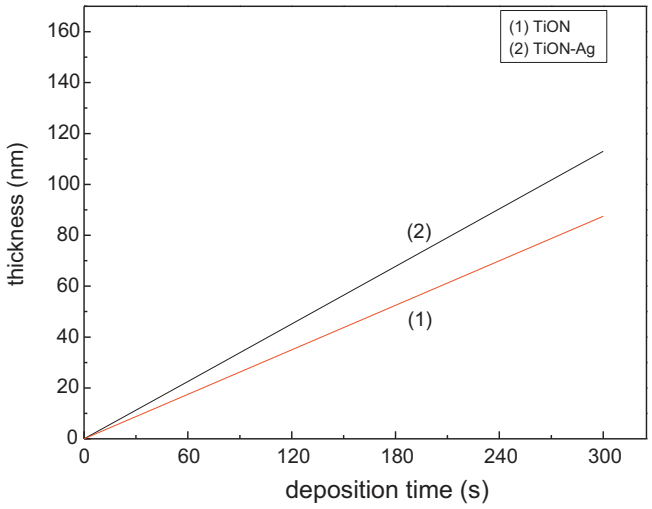

Fig. 2. Thickness of TiON(1) films and TiON-Ag (2) films as a function of DC-magnetron sputtering time. Reactive gas flow composition: Ar 90%:$N_2$5%:510% and total P 0.5 Pa. For other details see text.

OMCL-TR400 with a spring constant 0.02 N/m. Images with a scanning field 600 nm × 600 nm microns were taken using a line frequency 2 Hz. The roughness was calculated using Parks' XEI software. The contact angle (CA) of TiON and TiON-Ag was determined by the sessile drop method on a DataPhysics OCA 35 unit.

2.7. Zeta potential (z) determination of protein size and inductively coupled plasma mass-spectrometry (ICP-MS)

This approach investigated the residual protein attached to the film surface in contact with the bacteria during the course of bacterial inactivation. The Malvern Zetasizer Nano-Z system measured the zeta potential and electrophoretic mobility using Laser Doppler Micro-Electrophoresis and dynamic light scattering. The results were processed by a Zetasizer version 6.32 software. The Finnigan^{TM}ICP-MSS instrument used was equipped with a double focusing reverse geometry mass spectrometer presenting an extremely low background signal and high ion-transmission coefficient. The spectral signal resolution was 1.2×10^5 cps/ppb and the detection limit of 0.2 ng/L.

2.8. X-ray photoelectron spectroscopy (XPS)

An AXIS NOVA photoelectron spectrometer (Kratos Analytical, Manchester, UK) equipped with monochromatic AlK_α ($h\nu$ = 1486.6 eV) anode was used during the study. The carbon C1s line with position at 284.6 eV was used as a reference to correct the charging effects. The surface atomic concentration of some elements was determined from peak areas using known sensitivity factors [33]. Spectrum background was subtracted according to Shirley through the Shirley subtraction GL(30) program of the Kratos unit [34]. The XPS spectra for the Ag-species were analyzed by means of spectra deconvolution software (CasaXPS-Vision 2, Kratos Analytical, UK).

3. Results and discussion

3.1. Ti and Ag deposition rate, O_2/N_2 ratio and thickness calibration

Fig. 1 shows the atomic deposition rate of TiON films as a function of the O_2/N_2 ratio. The total pressure $P_T = (P_{Ar} + P_{N_2} + P_{O_2})$ was fixed at 0.5 Pa and after optimization the fastest bacterial inactivation kinetics and consisted of a gas flow Ar 90%:N_2 5%:O_2 5%.

The thickness calibration of the TiON layers was carried out on silica wafers sputtering up to 5 min in a gas flow Ar 90%:N_2 5%:O_2 5% and the results are shown in Fig. 2. The film thickness was determined with a profilometer (Alphastep500, TENCOR) and the data in Fig. 2 were in error by ±10%. Sputtering for 4 min lead to layers ~70 nm thick. This is equivalent to 350 layers each containing 10^{15} atoms/cm^2 being deposited at a rate of ~1.5×10^{15} atom/cm^2 s [32]. Fig. 2 shows TiON-Ag layers with a thickness of 90 nm after sputtering TiON for 4 min, followed by Ag-sputtering for 30 s. This led to an Ag-layer of ~20 nm with an Ag- atomic rate of deposition of 3.3×10^{15} atoms/cm^2 s. The atomic deposition rate has been reported to be a function of the O_2/N_2 ratio by several laboratories [19,20,25–28].

The colors of the TiON samples sputtered for 4 min are shown in Fig. 3, row A these colors are seen to be a function O_2/N_2 ratio. The collective oscillations of the electron plasmons in the TiON show a darker color for a higher ratio O_2/N_2. The visible light photocatalysis mediated by TiON has been suggested to require a certain ratio of N_2/O_2 [35–37]. The color is due to the N-doping of the TiO_2-lattice [36] inducing interstitial N-doping in the TiO_2 accompanied by the formation of O-vacancies. This leads to charge transfer states responsible for the TiON absorption in the visible region [37]. A

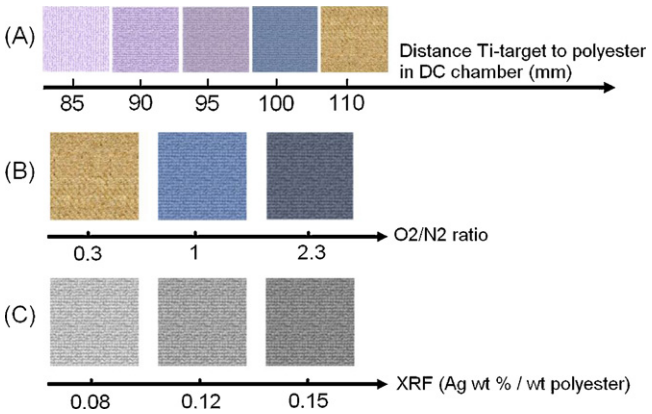

Fig. 3. Visual presentation of the samples of sputtered TiON and TiON-Ag textiles within 4 min: (A) color variation as a function of the distance of the Ti-target and the polyester sample, (B) color variation as a function O_2/N_2 ratio for TiON samples, (C) color variation of TiON-Ag samples with different Ag wt%/wt polyester.

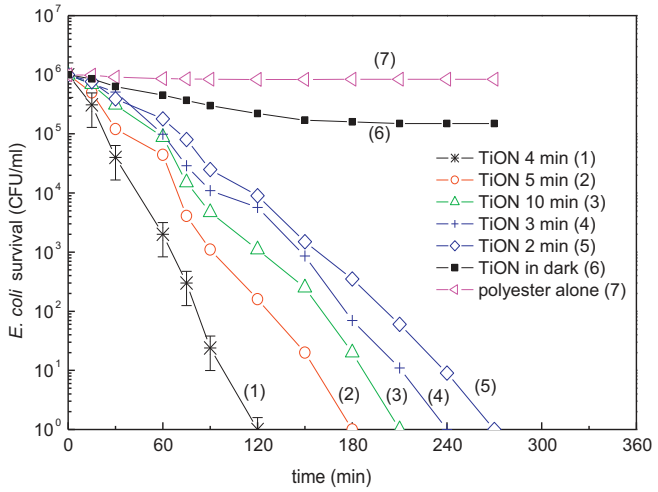

Fig. 4. *E. coli* survival on polyester sputtering TiON for: (1) 4 min, (2) 5 min, (3) 10 min, (4) 2 min, (5) 1 min, (6) TiON 4 min in dark and (7) polyester alone. The light source is an Osram lamp L18W/827 (4 mW/cm^2, 400–700 nm). Reactive gas flow composition: Ar 90%:$N_2$5%:$O_2$5% and total P 0.5 Pa.

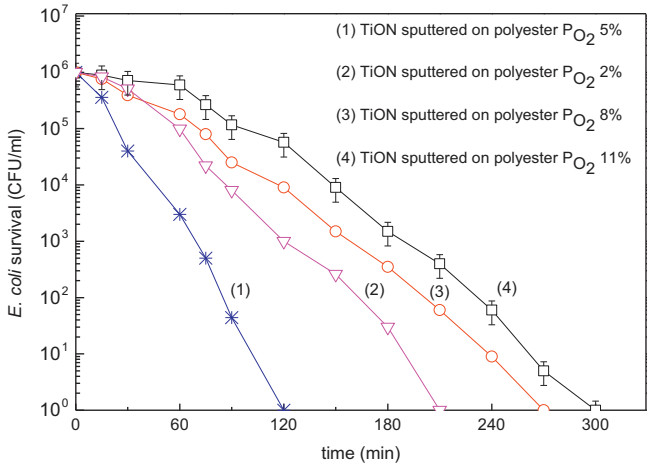

Fig. 5. *E. coli* survival on TiON–polyester sputtered (4 min) for different oxygen flow-rates. Reactive gas flow composition: Ar 90%:$N_2$5%:$O_2$5%. The light source is an Osram lamp L18W/827 (4 mW/cm^2, 400–700 nm).

higher content of O_2 has been reported to increase the biocompatibility of the TiON samples [1,35].

The samples TiON 4 min sputtered with Ag for 20–40 s in Fig. 3(B) and became darker for TiON samples sputtered for longer times. The wt% Ag/wt polyester of the TiON-Ag samples sputtering Ag for 20, 30 and 40 s are shown in Fig. 3(C). The color darkening is due to the increased amount of Ag-deposited at longer sputtering times leading to stronger inter-particle coupling of the Ag-particles though the formation of higher aggregates leading to a darker Ag-absorption band. These bands were also determined by diffuse reflectance spectroscopy (DRS) are later shown in Fig. 9.

Table 1 shows the weight percentages of Ag and Ti in the TiON and TiON-Ag samples. The kinetically fastest bacterial inactivation sample TiON-Ag (4 min–30 s) had a 0.25 wt% Ti/wt polyester and an Ag-content of 0.021 wt% Ag/wt polyester.

3.2. Inactivation kinetics of E. coli on TiON-sputtered samples

Fig. 4 shows the bacterial inactivation kinetics as a function of the TiON sputtering on polyester for times between 2 and 10 min time under low intensity visible light irradiation. Samples in trace (1) sputtered for 4 min seem to contain the optimal coverage of TiON to absorb all the incoming light and generate charges in the TiO_2 as shown in the XPS section by deconvolution of the TiO_2 spectrum in the XPS TiON spectra. This sample shown in trace (1) presents the highest amount of active sites/carriers held in exposed interacting with the bacteria [15,16,29]. Films sputtered for 2 and 3 min and shown in traces (4, 5) do not contain enough TiON to drive a fast bacterial inactivation under light. Samples sputtered for 5 and 10 min as shown in traces (2, 3) seem to contain TiON layers with a thickness much above the above 70 nm found for the sample sputtered for 4 min (trace 1). This leads to bulk inward diffusion of the charge carriers induced under light in TiON [6,32]. These charge carriers are responsible for the electrostatic attraction between the TiON film and bacteria.

Fig. 5 shows the effect of the amount of O_2 in the reactive gas composition when sputtering for 4 min TiON on polyester. The results reveal the strong dependence of the bacterial inactivation kinetics on the O_2% in the flow gas composition. The oxygen concentration of the TiON samples has been reported as one of the most important factors affecting the photocatalytic performance of TiON films [26,27] due to the fact that different O_2 concentrations in the gas flow introduce a different amount of oxygen vacancies. These vacancies lead to charge transfer states determining the photocatalytic activity [36,37].

Fig. 6 shows the bacterial inactivation of *E. coli* by TiON-Ag films. The TiON layers were sputtered for 4 min and the Ag-sputtering was applied sequentially up to 40 s. A small bacterial inactivation was observed in the dark (Fig. 6, trace 5) possibly due to adsorption of *E. coli* on the polyester, since Ag-ions are shown in this study to be produced under light irradiation on the TiON-Ag-films. The bacterial inactivation kinetics increases as the Ag sputtering time was increased from 10 to 30 s attaining a maximum at 30 s due to the known bactericide properties of Ag [14–17,21–23]. The inactivation kinetics falls back at 40 s possibly due to the formation of bigger Ag-clusters [17,18,29,30] hindering electron injection from Ag/Ag_2O into TiO_2 [19,20]. The Ag-clusters are not necessarily crystalline and darken the polyester samples as a function of sputtering time [38].

The *E. coli* survival on Ag-sputtered directly on the polyester fabric led to longer inactivation times of 1 $\log_{10}$, 2 $\log_{10}$ and 3 $\log_{10}$ for sputtering times of 10, 20 and 30 s (data not shown). The 6 $\log_{10}$ bacterial inactivation time of 55 min shown in Fig. 6 for TiON-Ag (4 min–30 s) samples is possible since the TiON smooth thin layer on the polyester merges without forming boundaries with the polyester [32]. On the TiON coating, a topmost Ag-layer immiscible with TiON was observed and is shown below in the EM section.

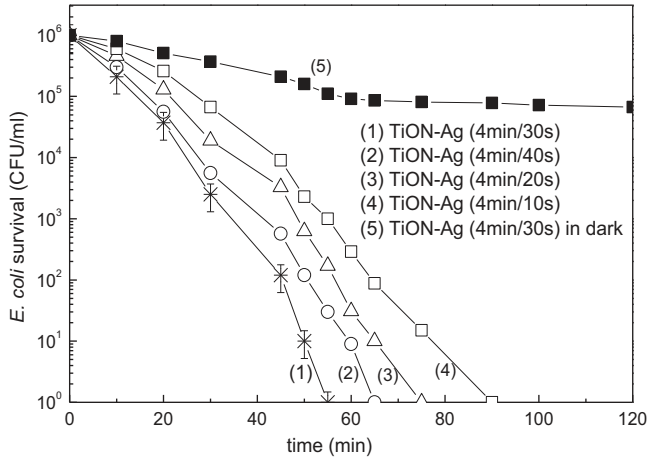

Fig. 6. *E. coli* survival on TiON-Ag sputtered on polyester for different Ag deposition times on TiONlayers. The light source is an Osram lamp L18W/827 (4 mW/cm^2, 400–700 nm). Reactive gas flow composition: Ar 90%:$N_2$5%:$O_2$5% and total P 0.5 Pa.

Table 1
X-ray fluorescence (XRF) of Ag, TiON and TiON-Ag sputtered on polyester.

Samples sputtered on polyester	%wt Ag/wt polyester	%wt Ag_2O/wt polyester	%wt Ti/wt polyester	%wt TiO_2/wt polyester
Ag (20 s)	0.08	0.08	–	–
Ag (30 s)	0.12	0.13	–	–
Ag (40 s)	0.15	0.17	–	–
TiON (4 min)	–	–	0.27	0.39
TiON-Ag (4 min/30 s)	0.021	0.023	0.25	0.26
TiON-Ag (4 min/40 s)	0.024	0.029	0.24	0.26

3.3. Effect of light intensity on the inactivation kinetics and recycling of TiON-Ag samples

Fig. 7(A) presents the bacterial inactivation kinetics mediated by TiON-Ag (4 min–30 s) polyester samples applying different light doses. It is readily seen that the bacterial inactivation kinetics by the TiON samples are strongly dependent on the light dose in the reactor cavity. The same trend was observed for the TiON-Ag samples in Fig. 7(B). This up-to-date actinic light is currently used in hospital facilities in Switzerland.

Fig. 8(A) presents the TiON-Ag (4 min–30 s) inactivation of *E. coli* up to the 8th, repetitive recycling. After each 55 min cycle, the sputtered polyester fabrics were washed thoroughly with sterilized MQ-water, vortexed for 3 min and dried at 80 °C to be sure that no bacterial remained on the polyester. Then the fabric was reused with a small decrease in the bacterial inactivation kinetics and washed thoroughly after each run. An increase in the *E. coli* inactivation of less than 15% is observed as the cycling number increases due to the loss of Ag [22]. Silver ions seem to be toxic to bacteria as documented in Fig. 8 via the oligodynamic effect. The samples released after 8 cycles less than 10 ppb/cm^2 of Ag as shown later in this study by ICP-MS in Fig. 14(a). The Ag level in solution determined by ICP-MS is well below standards established for the Ag cytotoxicity for a several of living organisms [1,2,10].

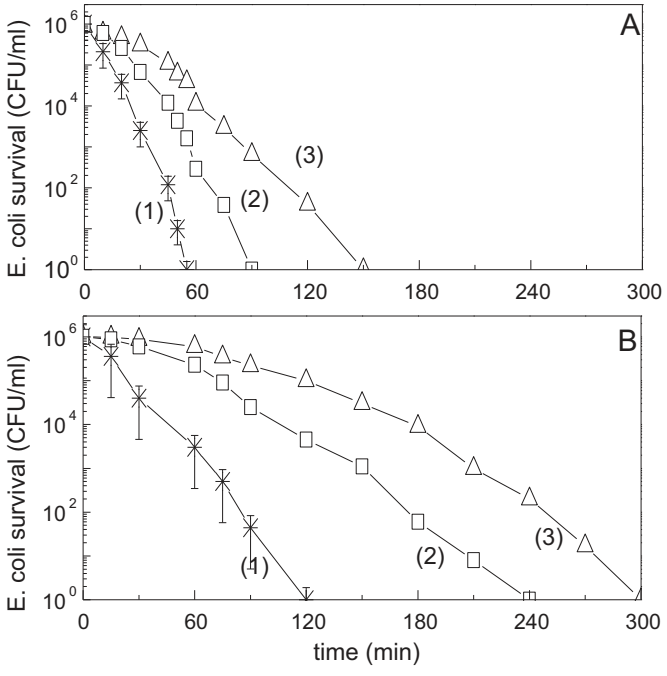

Fig. 7. *E. coli* survival on: (A) TiON-Ag sputtered on polyester(4 min–30 s) irradiated with an Osram Lumilux light source (400–700 nm) 18 W/827 at different light doses: (1): 4 mW/cm^2, (2): 2.5 mW/cm^2, (3): 1 mW/cm^2; (B) TiON sputtered on polyester(4 min) and irradiated with an Osram Lumilux light source (400–700 nm) 18 W/827 with different light doses: (1): 4 mW/cm^2, (2): 2.5 mW/cm^2, (3): 1 mW/cm^2. Reactive gas flow composition: Ar 90%:N_2 5%:O_2 5% and total P 0.5 Pa.

Fig. 8(B) presents data up to the 8th recycling indicating a more significant increase in the bacterial inactivation time with the number of cycles for the TiON samples. TiON-polyester samples should be used when Ag leaching represents a potential environmental danger although their kinetics is slower compared to the TiON-Ag samples (Fig. 8). The cause for the slower inactivation kinetics upon repetitive recycling of the TiON photocatalysts has not been determined in this study.

3.4. Diffuse reflectance spectroscopy (DRS) and visual appearance of sputtered samples

Fig. 9(A) and (B) shows the increased spectral absorption for the TiON-Ag and Ag-polyester samples with longer sputtering times. The shapes of the DRS spectra reflect differences in particle size, particle surface density and the coupling between Ag and the TiON nanoparticles. The TiON layers dielectric confinement has been reported to shift the Ag-spectra to the red [19,20]. A lower absorption was observed when Ag was sputtered directly on polyester (Fig. 9(B)). The formation of a Schottky barrier has been reported for Ag on semiconductor surfaces promoting charge separation in Ag/Ag_2O [39,40], and may account for the better bacterial inactivation performance of the TiON-Ag samples (Fig. 6) compared to the TiON samples (Fig. 4).

3.5. Sample transmission electron microscopy (TEM) and atomic force microscopy (AFM)

Fig. 10(a) presents in the left hand side the almost continuous dark TiON-Ag (4 min–30 s) deposit on the polyester fiber.

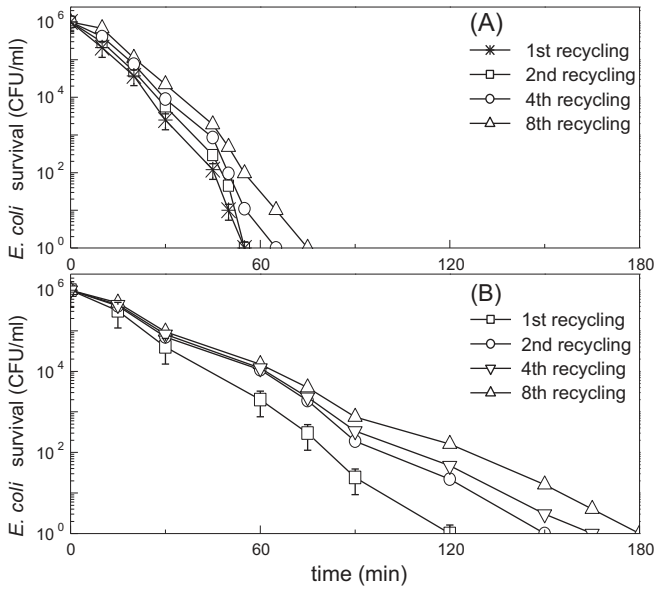

Fig. 8. (A) Recycling of TiON-Ag (4 min–30 s) Sputtered samples inactivating bacteria for the 1st, 2nd 4th and 8th cycle, (B) recycling of TiON 4 min sputtered samples for the 1st, 2nd 4th and 8th cycle inactivating bacteria.

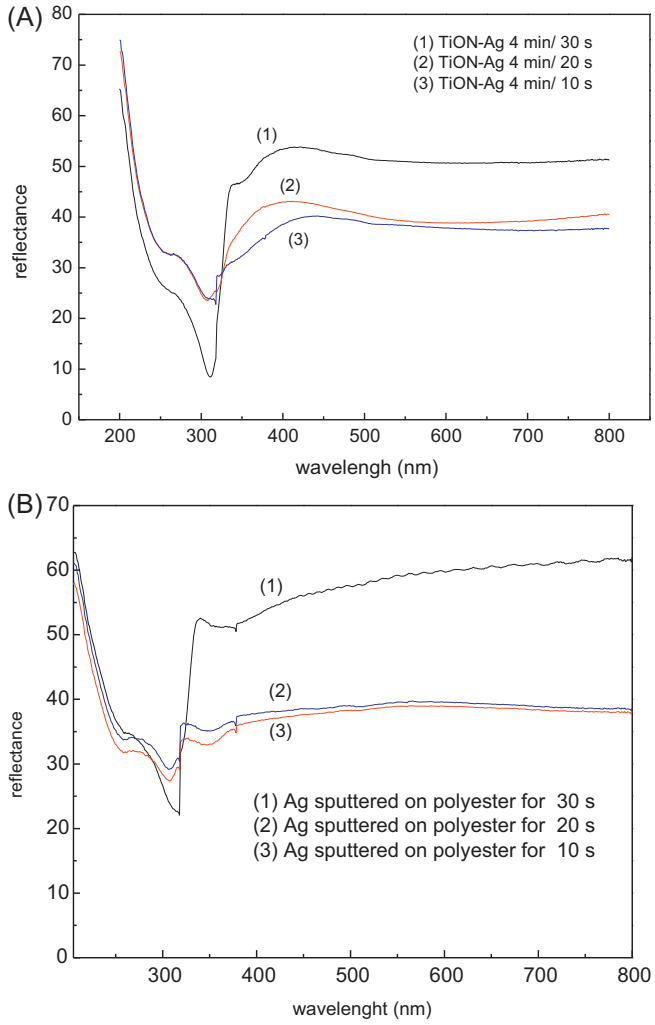

Fig. 9. (A) Diffuse reflectance spectra of TiON4 min sputtered samples sputtering subsequently Ag for 10 s, 20 s and 30 s, (B) Diffuse reflectance spectra of polyester sputtered-Ag samples for with 10 s, 20 s and 30 s.

The right hand side image with a bigger magnification of 100 nm shows the immiscibility of the Ag-dark coating and the TiON coating gray layers. The Ag-particles present sizes between 20–40 nm within a TiON-Ag layer with a width of 70 ± 10 nm. Ag/Ag_2O particles of 20–40 nm will no permeate through the bacterial cell wall having protein porin pores with a diameter of 1.1–1.5 nm [1,7,15]. This confirms one more that Ag bacterial inactivation goes by the Ag-ions having sizes <1 nm, and not Ag-nanoparticules.

Fig. 10(b) shows the image of a TiON-Ag (4 min–30 s) sample in bright field (BF). The immiscibility of the Ag and Ti on the sample surface is readily seen at the current beam position.

Fig. 11(A) shows the atomic force microscopy of TiON sputtered for 4 min. The TiON grains 70–100 nm in size lead to a rugosity value (rms) of 0.33 nm. The focal field of 600 nm × 600 nm is able to provide for a low-resolution image. The rms values found indicated low surface rugosity (<2.5 nm) and therefore it is unlikely that the roughness variation between the samples will have a significant effect on the contact angle measurements as addressed below. Fig. 11(B) shows grains 100–400 nm in size for TiON-Ag (4 min–30 s) samples. Ag is seen to compact the TiON surface grains and increases the rms of TiON-Ag (4 min–40 s) value to 1.48 nm.

Table 2
Surface percentage atomic concentration of elements during *E. coli* inactivation on TiON-Ag polyester (4 min/30 s) sputtered samples under Osram Lumilux light (400–700 nm) 4 mW/cm^2.

	O1s	Ti2p	N1s	Ag3d	C1s
$t = 0$	7.13	2.04	4.47	21.50	23.71
$t = 0$ contacted bacteria	7.15	2.01	4.44	21.50	23.70
$t = 30$ min	9.09	2.51	3.02	23.11	34.22
$t = 55$ min	12.55	2.66	2.47	23.29	44.76

3.6. Contact angle (CA) changes during bacterial inactivation

It is not possible to follow in the time scale the decrease of the CA for a water droplet on the polyester fabric since the droplet disappears instantly by contact with the fabric. Although the polyester is hydrophobic by nature, the high porosity of the polyester promotes instantly the droplet penetration through the polyester microstructure. This porosity (void areas) in the polyester is significantly reduced due to the sputtering of TiON or Ag or both, decreasing the surface water penetration concomitantly increasing the sample hydrophobicity.

Fig. 12 shows in trace (1) the CA for a water droplet on a TiON-polyester sample sputtered for 4 min reaching zero degrees after 30 min. Traces (2)–(5) show the progressive increase in the initial CA for 4 min sputtered TiON samples Ag-sputtered from 10 s up to 40 s. An increase in the surface hydrophobicity due to the Ag-sputtering is detected. Trace 6 shows the CA for the TiON-Ag (4 min–30 s) sample upon contact with bacteria, disappearing completely within 55 min. The increase in the hydrophobicity of the TiON-Ag (4 min–30 s) sample (trace 6) to 117° was due to the adsorbed bacteria on the sample surface. The bacterial bilayer envelope contains hydrophobic groups such as: (a) phosphatidyl-ethanolamine (PE), (b) lipid polysaccharide (LPS) and (c) peptoglycan [41,42]. The surface of the TiON-Ag (4 min–30 s) sample was therefore to be weakly hydrophobic.

The zero CA reached on the TiON-Ag (4 min–30 s) sample within 55 min in Fig. 12 implies self-cleaning of any hydrophobic residue at the end of the bacterial inactivation. The XPS data in Table 2 shows the atomic percentage surface concentration of N-, Ti and Ag- for this sample being almost constant up to the end of the bacterial inactivation. The N- coming from the residual bacteria fragments is quickly destroyed on the photocatalytic film under light irradiation. Furthermore, the constancy of the atomic concentration of Ag and Ti in Table 2 shows evidence for Ag-sites not being blocked during bacterial inactivation [6,17,18]. This observation means that at the end of the inactivation process, the sample being free of hydrophobic compounds is ready to inactivate a new bacterial charge with the kinetics observed in the first bacterial inactivation cycle (Fig. 8).

3.7. Protein size and ion-release during bacterial inactivation by small angle laser scattering and ICP-MS.

Zeta-potential analysis was used to determine the sizes of the residuals protein fragments left on a TiON-Ag (4 min–30 s) sample contacted with bacteria under visible light irradiation. The Malvern Zetasizer series combines a particle size analyzer, a zeta potential analyzer and a molecular weight analyzer for particles measuring less than one nanometer up to several microns. This determination is based on the amount of light scattered and particle charge by the fragments on the photocatalyst at different inactivation times. The over tenfold reduction in size reported in Fig. 13 decreasing to very small sizes shows that degradation of the protein residues.

This is a further evidence for the self-cleaning occurring on the TiON-Ag (4 min–30 s) sample. The TiON-Ag sample inactivates *E. coli* bacteria and reduces the protein sizes beyond the 55 min period necessary to inactivate completely the bacteria.

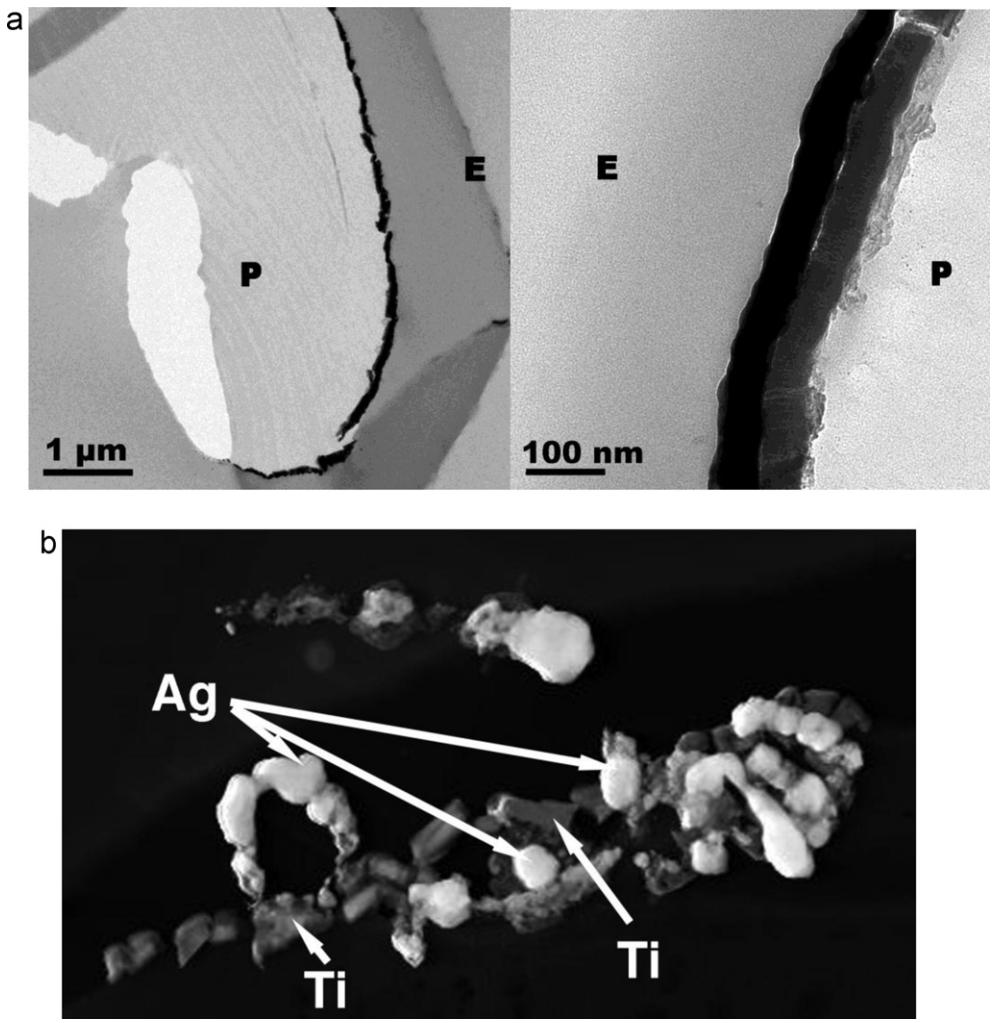

Fig. 10. (a) Left hand side: Transmission electron microscopy of a TiON-Ag (4 min-30 s) DC-sputtered sample showing the continuity of the sputtered TiON-Ag layer around the polyester fiber. Right hand side: the same sample showing with a bigger magnification the darker continuous Ag-layers being immiscible with the gray TiON layer (P = polyester and E = epoxide). (b) Image of the sample TiON-Ag (4 min–30 s) in bright field (BF) showing the surface elements at the current beam position.

The bacterial fragment >55 min attains the small size ~78.8 nm as shown in Fig. 13, less than 10% of its initial size. It is possible that the protein was degraded as shown in Fig. 13, but that the amount of protein did not change significantly. Again it has not to be overlooked that self-cleaning is due to light irradiation as shown below in Fig. 17.

Fig. 14 presents the release of Ti and Ag up to the 8th recycling during bacterial inactivation runs. The results for samples of TiON, TiON-Ag and Ag are shown in Fig. 14. Fig. 14(a), trace 1 shows the slow release of Ti up to the 8th recycling from the TiON 4 min sample. Trace 2 shows the Ag-ion release starting at a level of 6 ppb/cm^2 for TiON-Ag (4 min–30 s) sample and reaching ~5 ppb/cm^2 on the 8th recycling. Ag-ions are formed by oxidation of the Ag on the polyester in the reaction media. Ag-ions with a concentration >0.1 ppb show a significant antimicrobial activity. Higher Ag-ion concentrations >35 ppb can be toxic to human cells [1]. The antimicrobial performance of Ag is dependent on the oxidation state of the Ag-ion [14] as identified by XPS (see Table 3). Fig. 14(a); trace 3 shows the release of Ag-ions sputtered for 30 s on polyester. A high level of Ag-ions at time zero reaches on the 8th recycling about the same level as the Ag-released by the TiON-Ag (4 min–30 s) samples. The biocompatibility of TiON has been well documented in biomedical applications [1,24,26,35]. The TiON fast inactivation kinetics and a concomitant low cytotoxicity are the two essential requirements for the application of these antibacterial surfaces. Long-term performance and cytotoxicity studies of TiON samples are under way in our laboratory.

Fig. 14(b) presents the release of Na^+ and K^+ during the bacterial inactivation from a TiON-Ag (4 min–30 s) sample under Osram Lumilux light. The K^+-ion exists universally in bacteria regulating the potential for the transfer of ions across the bilayer membranes [42]. The K-ions leak at a low rate from the bacterial cell as the cell membrane becomes more permeable up to 30 min reaching a relatively low value [43]. The Na^+-ions in Fig. 14(b) are seen to leak at a faster rate compared to K^+-ions due to their smaller size compared to the K^+-ions. The leakage of K^+ and Na^+ increases after 30 min due to the more advanced state of decomposition of the cell bacterial envelope [41,42,44]. The loss of cell viability shown in Fig. 6 within ~55 min, is consistent with the decomposition of the cell-wall membrane and the time of the leakage of intracellular K^+ and

Table 3
Auger lines of Ag and Ag sputtered on TiON-polyester (Reference values: Ag^0 725.15 eV, Ag(I) 725.53 eV, Ag(II) 725.66 eV).

Sputtering time	Ag polyester (eV)	Ag TiON polyester (eV)
10 s	725.14	725.15
20 s	725.15	725.53
30 s	725.53	725.55
40 s	725.53	725.67

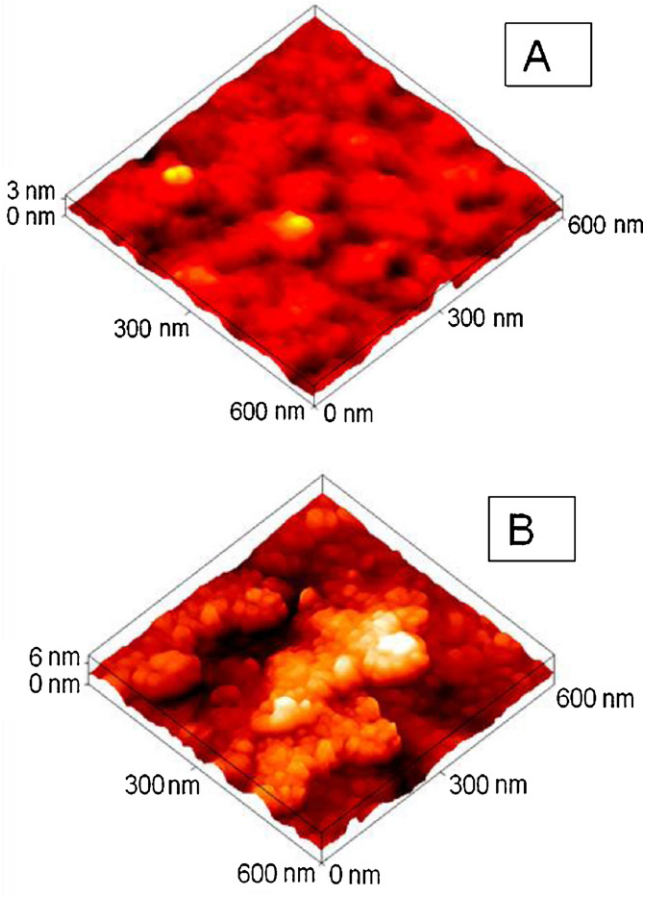

Fig. 11. (A) Atomic force microscopy (AFM) of TiON sputtered on Si-wafers for 4 min, (B) atomic force microscopy (AFM) of a TiON-Ag (4 min–30 s) sputtered on Si-wafers.

Na^+ shown in Fig. 14(b). The protein leakage shown in Fig. 13 indicates the efflux of protein is not proportional to the cell viability (see Fig. 6) or the K^+, Na^+ leakage (Fig. 14(b)) since the rate of disruption of *E. coli* cell wall is lower than that of the cell inactivation. The damages to the cell wall are repaired during the culture of cells on the agar plates. This leads to a different rate of decomposition of the outer cell membrane [45].

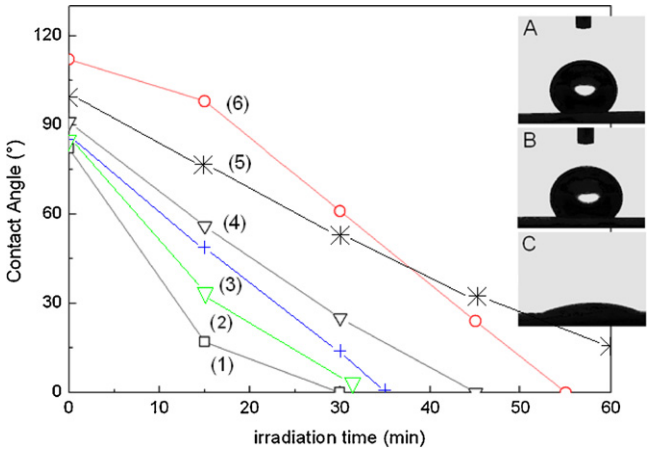

Fig. 12. Initial contact angle of samples; trace (1) TiON (4 min), trace (2) TiON-Ag (4 min–10 s), trace (3) TiON-Ag (4 min–20 s), (4) TiON-Ag (4 min–30 s), (5) TiON-Ag (4 min–40 s) and (6) TiON-Ag (4 min–30 s) contacted with bacteria for 3 s as a function of irradiation time. Light source Osram Lumilux L18 W/827 (4 mW cm^2, 400–700 nm).

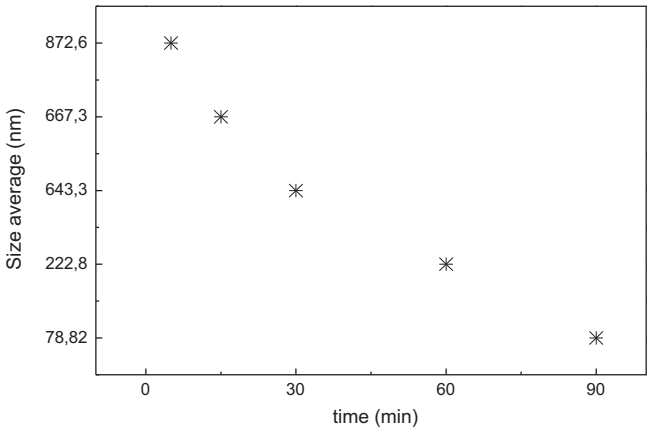

Fig. 13. Reduction in the protein size determined by small angle laser scattering as a function of irradiation time by a Osram Lumilux light source (400–700 nm) 18 W/827 on a TiON-Ag (4 min–30 s) sample contacted with bacteria.

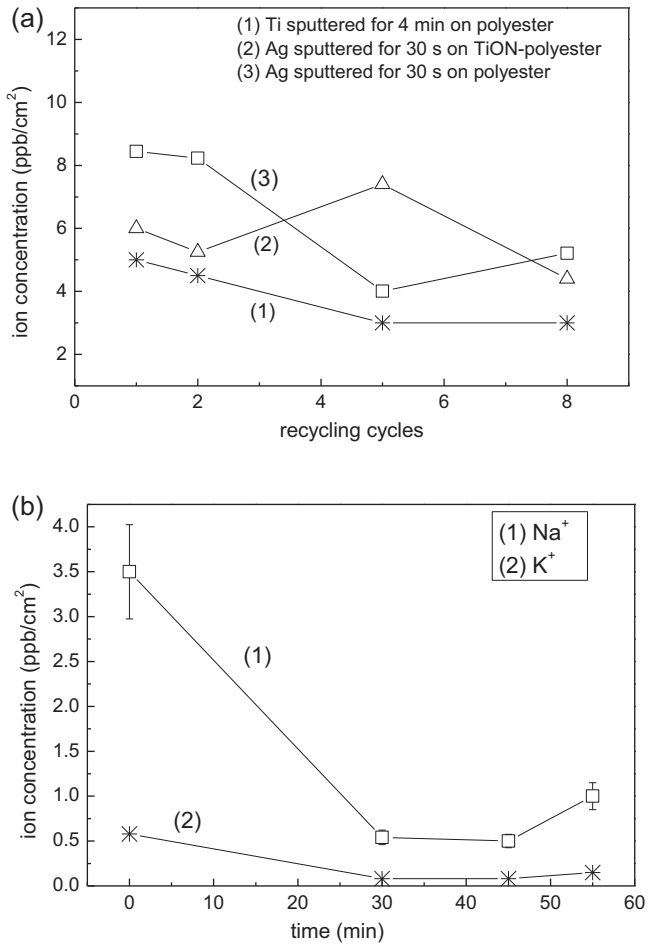

Fig. 14. (a) Ion-coupled plasma spectrometry (ICPS) determination of Ag ions and Ti-ions released during the recycling of (1) TiON sputtered 4 min on polyester, (2) a TiON-Ag (4 min–30 s) polyester sample and (3) a sample of Ag-polyester sputtered 30 s. (b) Ion-coupled plasma mass spectrometry (ICP-Ms) determination of the leakage of (1) Na^+ and (2) K^+-ions through the *E. coli* cell-wall envelope during bacterial inactivation by a TiON-Ag (4 min–30 s) sample irradiated by an Osram Lumilux light source.

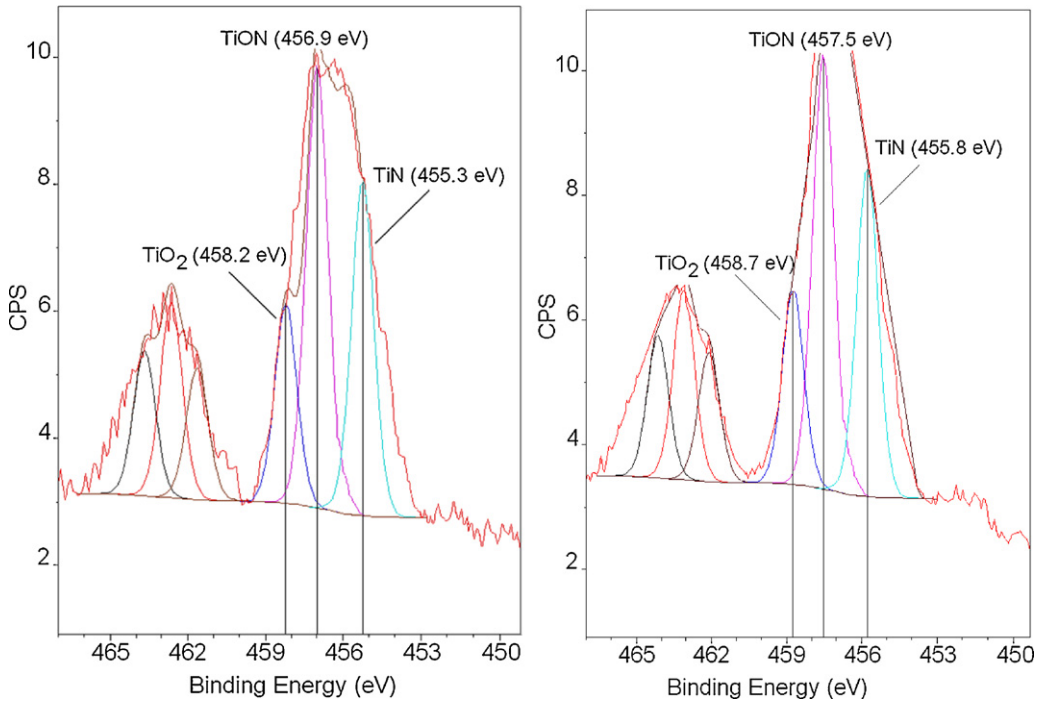

Fig. 15. XPS of the Ti2p3/2 peak showing the TiN, TiON and TiO_2 on the DC-sputtered TiON-Ag (4 min–30 s) samples at time zero (left-hand side).

3.8. X-Ray photoelectron spectroscopy (XPS)

Fig. 15 (left-hand side) presents the XPS spectra TiON-Ag (4 min–30 s) at time zero. The figure in the right-hand side presents the XPS for TiON-Ag (4 min–30 s) contacted 3 s with bacteria. The TiON species shows a peak at 456.9 eV, the TiO_2 peak ($Ti2p_{3/2}$) at 458.2 eV and the TiN peak at 455.3 eV [33]. Fig. 15 presents evidence for TiO_2 when TiON is reactively sputtered on polyester as described in Section 2.

Fig. 15 (right-hand side) presents the $Ti2p_{2/3}$ peak to 458.7 eV indicating a slight shift of this peak due to Ti^{3+}/Ti^{4+} redox reactions on the sample surface. Shifts of the TiON and TiN peaks are also observed in the right-hand side of Fig. 15, providing further proof for redox reactions during the bacterial inactivation. Shifts in the XPS peaks $\geq$0.2 eV reflect valid changes in the oxidation states of the elements [34].

Fig. 16(a) shows the $Ag3d_{5/2}$ peak shift from 364.4 eV to 365.2 eV when sputtering Ag from 10 s up to 40 s on a sample previously sputtered with TiON. The position of the Ag Auger lines for the TiON-4 min samples sputtered with Ag for 10 s up to 40 s is shown in Table 3 [14,33]. The shift of the Auger lines from 725.15 to 725.65 eV indicates an increasing amount for Ag^+/Ag^{2+}-ions at longer sputtering times. The fastest bacterial inactivation seems to be due to the TiON-Ag (4 min–30 s) samples containing Ag^{2+} ionic-species suggesting that the bactericide activity is due to higher Ag-ionic species [14].

The data obtained by XPS above for the Ag-ions intervening in bacterial inactivation using TiON-Ag (4 min–30 s) allows to relate: (a) the nature of the most favorable Ag-ions in the TiON-Ag samples with (b) the kinetics of bacterial inactivation presented for this sample in Fig. 6(b), with (c) the rugosity of the sample described above in Fig. 11, and finally with (d) the CA values found for the samples in Fig. 12. The TiON-Ag (4 min–30 s) sample shows a significant amount of Ag^{2+} as detected by XPS in Table 3, leading to a fast bacterial inactivation time of 55 min (Fig. 6), showing a rugosity of 1.48 nm and a CA of 90° presenting the best hydrophobic/hydrophilic balance for a fast bacterial inactivation. The bacterial inactivation time by the later sample is in the range reported for *E. coli* inactivation by Ag_2O/TiON suspensions under halogen lamp irradiation [46–48]. These samples lead to bacterial inactivation within minutes needing a shorter time compared to the inactivation times reported for TiO_2 films and oxynitrides [49].

Fig. 16(b) shows the $Ti2p_{3/2}$ shift from 457 eV and 458.1 eV within 55 min during *E. coli* inactivation providing the evidence for Ti^{4+}/Ti^{3+} redox processes taking place on the polyester surface.

Fig. 16(c) shows the Ag-oxidation states shifting within the bacterial inactivation time. Higher Ag-oxidation states have been reported to be beneficial reducing within the bacterial inactivation time [14].

Fig. 16(d) shows the O1s peak shift between time zero and 55 min during *E. coli* inactivation. The XPS-signal increases due to O-rich functionalities C—OH, C—O—C and carboxyl species [18] origination from the bacterial oxidation on the catalyst surface. Table 2 shows the surface atomic composition percentage for the main elements of TiON-Ag (4 min–30 s) polyester as a function of the bacterial inactivation time. The composition of the ten upper layers (2 nm) at time zero for the TiON-Ag (4 min–30 s) sample is: $Ti_{0.06}O_{0.20}N_{0.13}Ag_{0.61}$. The surface atomic concentration for the O1s signal increases with bacterial inactivation time due to the oxidative residues produced during bacterial oxidation. The $Ti2p_{2/3}$ signals remain fairly constant indicating a rapid removal of the bacterial residues on the catalyst surface during the bacterial inactivation process. The almost constant amount of the surface N and Ag suggests an effective surface catalysis destroying bacterial residues during *E. coli* inactivation. The C1s signal is seen to increase with the bacterial inactivation time due to the adventitious hydrocarbons being spontaneously adsorbed from ambient air on the sample surface.

3.9. Mechanistic considerations

The TiON-Ag (4 min–30 s) as described in the preceding XPS section identifying the TiO_2 and TiN peaks. The Ag in the TiON-Ag (4 min–30 s) film forms AgOH on the film surface in contact

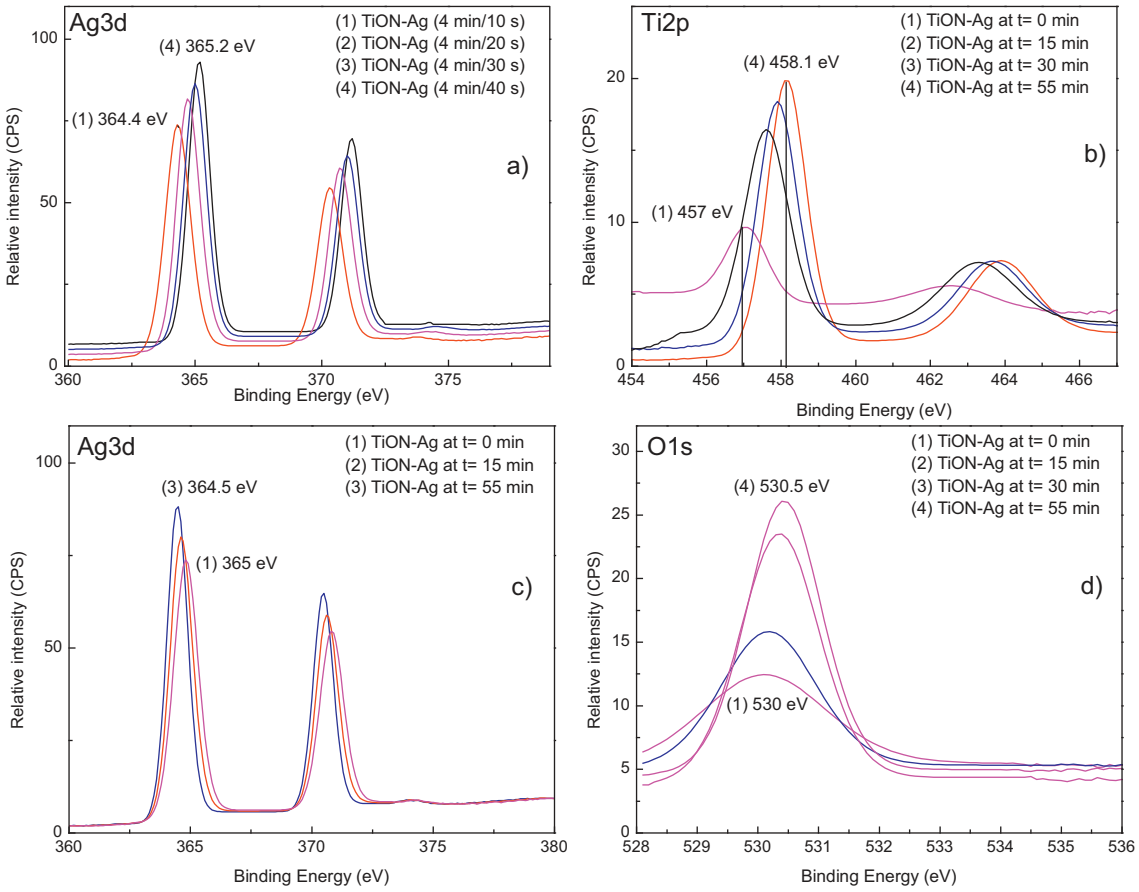

Fig. 16. (a) Ag3d5/2 shift during *E. coli* inactivation up to 55 min on TiON sputtering Ag for different times, (b) Ti2p3/2 shift during *E. coli* inactivation up to 55 min on TiON-Ag (4 min–30 s), (c) Ag3d5/2 during *E. coli* inactivation up to 55 min on TiON (4 min–30 s), (d) O1s shift between during *E. coli* inactivation up to 55 min on TiON-Ag (4 min–30 s).

with air. The AgOH decomposes spontaneously to Ag_2O (Eq. (1)) [50]

$$2AgOH \rightarrow Ag_2O + H_2O(pk = 2.87) \quad (1)$$

This Ag_2O is stable in the thermodynamically stable region at pH 6–7 where the bacterial inactivation of *E. coli* proceeds. Visible/actinic light irradiation photo-activates Ag_2O with $1.46 < bg < 2.25$ eV [51,52] as noted next in Eq. (2)

$$Ag_2O + light \rightarrow Ag_2O(h^+) + Ag_2O(e^-) \quad (2)$$

The Ag_2O/TiO_2 transfer of charges we have to consider the position of the energy bands of Ag_2O and TiO_2. Under visible light irradiation, the transfer of charge from Ag_2O to TiO_2 is thermodynamically favorable because the position of the Ag_2Ocb −1.3 eV NHE at pH 0 and the vb of Ag_2O +0.2 V NHE at pH 0 [51–53] lies above the TiO_2cb at −0.1 V vs. NHE and the vb at +3.2 V [6]. The fast *E. coli* inactivation kinetics reported in Fig. 6 may be due to an interfacial charge transfer (IFCT) process between Ag/Ag_2O and TiON [53,54]. The Ag_2Ocb electrons transfer to the TiO_2cb in a downward energetic process as shown in Fig. 17 hindering the electron–hole recombination in the Ag_2O. We suggest that the increase in the transfer of the Ag_2O electrons to O_2 when electrons are injected into the TiO_2cb is the key to the increase the photocatalytic activity of the TiO_2 leading to bacterial inactivation (Fig. 17).

We suggest a mechanism in which the Ag_2O in Eq. (1) reacts with e^- as shown in Eq. (2) as seen next in Eq. (3)

$$Ag_2O + e^- \rightarrow 2Ag^\circ + \tfrac{1}{2}O_2^- \quad (3)$$

The O_2 in Eq. (3) would promote at later stages reactions ((5) and (6)) producing highly oxidative radicals, while the h^+ in Eq. (2) reacts with H_2O as suggested in Eq. (4). This reaction runs parallel with Eq. (5) generating OH° radicals or other highly reactive oxidative radicals by way of the Ag_2Ovb h^+ (see Eq. (2))

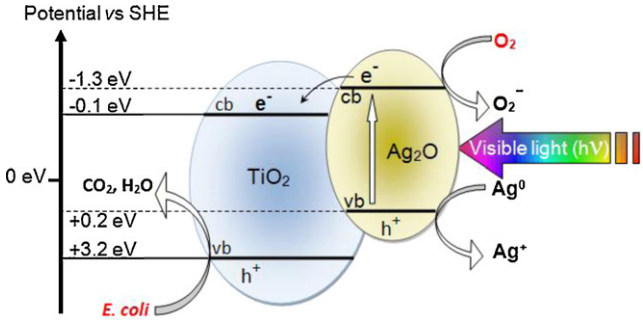

Fig. 17. Suggested reaction mechanism fir the visible light photo-induced electron injection by Ag_2O into TiO_2.

$$h^+ + H_2O \rightarrow OH^\circ + H^+ \quad (4)$$

$$2e^- + 2H_2O + O_2 \rightarrow 2OH^\circ + 2OH^- \quad (5)$$

$$e^- + O_2 \rightarrow O_2^{\bullet -} \quad (6)$$

4. Conclusions

TiON and TiON-Ag deposited on polyester by DC- and DCP-magnetron sputtering leading to thin uniform nanoparticulate films. The *E. coli* inactivation kinetics activated by visible light is reported in detail. The rapid destruction of the bacterial

decomposition residues during bacterial inactivation was detected by XPS. The lack of organic hydrophobic residues was shown by the zero CA attained after 55 min and also by Zetasizer protein size determination at the end of the bacterial inactivation. The correlation between the nature of the Ag-ions, the sample rugosity and the surface contact angle for the most effective bactericide TiON-Ag (4 min–30 s) sample is described. TiON-Ag is a faster inactivating catalyst compared to TiON, but as shown in this study by ICP-MS leaches out Ag-particles. The concentration found for silver particles were observed to be below the allowed cytotoxicity level for Ag as determined quantitatively in this study. Repetitive bacterial inactivation is reported was observed providing evidence for the stable nature of the photocatalyst. TiON on polyester is shown to be a suitable photocatalyst in the visible range inactivating bacteria within two hours and avoiding the leaching of the heavy metal Ag into the environment.

Acknowledgments

We thank the COST Action MP0804 Highly Ionized Impulse Plasma Processes (HIPIMS), the EPFL and the LIMPID 7 FEP Collaborative European Project Nanocomposite Materials for Photocatalytic Degradation of Pollutants NMP 2012.2.2.2-6 (no. 310177) for financial support of this work.

References

[1] Thüringer Surface and Biomaterials Kolloquium, 13–15 September, Zeulenroda, Germany, 2011.
[2] K. Taylor, R. Roberts, J. Roberts, The Challenge of Hospital Acquired Infections (HAI), National Audit Office, 2002.
[3] R. Plowman, R. Graves, N. Griffin, L. Taylor, The rate and cost of hospital acquired infections, Journal of Hospital Infection 47 (2001) 198–204.
[4] S. Dancer, The role of the environmental cleaning in the control of hospital acquired infections, Journal of Hospital Infection 73 (2009) 378–386.
[5] A. Kramer, I. Schwebke, G. Kampf, How long do nosocomial pathogens persist in on inanimate surfaces? BMC Infectious Diseases 6 (2006) 137–146.
[6] A. Mills, C. Hill, P. Robertson, Overview of the current ISO tests for photocatalytic materials, Journal of Photochemistry and Photobiology A 237 (2012) 7–23.
[7] K. Page, M. Wilson, P.I. Parkin, Antimicrobial surfaces and their potential in reducing the role of the inanimate environment in the incidence of hospital-acquired infections, Journal of Materials Chemistry 19 (2009) 3819–3831.
[8] S. Noimark, Ch. Dunnill, M.P. Wilson, I. Parkin, The role of surfaces in catheter-associated infections, Chemical Society Reviews 38 (2009) 3435–3448.
[9] C. Page, M. Wilson, N. Mordan, W. Chrzanowski, J. Knowles, P.I. Parkin, Study of the adhesion of *Staphylococcus aureus* to coated glass substrates, Journal of Materials Science 46 (2011) 6355–6363.
[10] K. Page, R. Palgrave, P.I. Parkin, M. Wilson, Sh. Savin, A. Chadwick, Titania and siver titania composite films on glass-potent antimicrobial coatings, Journal of Materials Chemistry 17 (2007) 95–104.
[11] H.A. Foster, P. Sheel, W.D. Sheel, P. Evans, S. Varghese, N. Rutschke, M.H. Yates, Antimicrobial activity of titatnia/silver and titania/copper films prepared by CVD, Journal of Photochemistry and Photobiology A 216 (2010) 283–289.
[12] M.S.P. Dunlop, P.C. Sheeran, A.J.M. Byrne, S.A. McMahon, M.A. Boyle, G.K. McGuigan, Inactivation of clinically relevant pathogens by photocatalytic coatings, Journal of Photochemistry and Photobiology A 216 (2010) 303–3010.
[13] M.H. Yates, A.L. Brook, B.I. Ditta, P. Evans, H.A. Foster, D.W. Sheel, A. Steele, Photo-induced self-cleaning and biocidal behviour of titania and copper oxide multilayers, Journal of Photochemistry and Photobiology A 197 (2008) 197–2008.
[14] I.M. Mejia, M. Marín, R. Sanjines, C. Pulgarín, E. Mielczarski, J. Mielczarski, J. Kiwi, Magnetron-sputtered Ag-modified cotton textiles active in the inactivation of airborne bacteria, ACS Applied Materials & Interfaces 2 (2010) 230–235 (and references therein).
[15] O. Baghriche, A. Ehiasarian, E. Kusiak-Nejman, A. Morawski, C. Pulgarin, R. Sanjines, J. Kiwi, Advantages of high power impulse magnetron sputtering (HIPIMS) of silver for improved *E. coli* inactivation, Thin Solid Films 520 (2012) 3567–3573.
[16] O. Baghriche, A. Ehiasarian, E. Kusiak-Nejman, A. Morawski, C. Pulgarin, R. Sanjines, J. Kiwi, High power impulse magnetron sputtering (HIPIMS) and traditional pulsed sputtering (DCMSP) Ag-surfaces leading to *E. coli* inactivation, Journal of Photochemistry and Photobiology A 227 (2012) 11–17 (and references therein).
[17] O. Baghriche, R. Sanjines, C. Ruales, C. Pulgarin, I. Stolitchnov, A. Zertal, J. Kiwi, Ag-surfaces sputtered by DC and pulsed DC-magnetron sputtering effective in bacterial inactivation: testing and characterization, Surface and Coatings Technology 206 (2012) 2410–2416.
[18] E. Kusiak-Nejman, A. Morawski, A. Ehiasarian, O. Baghriche, C. Pulgarin, E. Mielczarski, J. Mielczarski, A. Kulik, J. Kiwi, *E. coli* inactivation by high power impulse magnetron sputtered (HIPIMS) Cu-surfaces, Journal of Physical Chemistry C 115 (2011) 21113–21119.
[19] P. Kelly, H. Li, P. Benson, K. Whitehead, J. Verran, R. Arnell, I. Iordanova, Comparison of the tribological and antimicrobial properties of CrN/Ag, ZrN/Ag, TiN/Ag, and TiN/Cu nanocomposite coatings, Surface and Coatings Technology 205 (2010) 1606–1610 (and references therein).
[20] P. Kelly, H. Li, K. Whitehead, J. Verran, R. Arnell, I. Iordanova, A study of the antimicrobial and tribological properties of TiN/Ag nanocomposite coatings, Surface and Coatings Technology 204 (2009) 1137–1141.
[21] J. Thiel, L. Pakstis, S. Buzby, M. Raffi, M. Ni, J. Pochan, S. Shah, Antibacterial properties of silver-doped titania, Small 3 (2007) 799–803.
[22] L. Geranio, M. Heuberger, E. Nowack, The behavior of silver nano textiles during washing, Environmental Science and Technology 43 (2009) 8113–8118.
[23] T. Benn, P. Westerhoff, Nanoparticle silver released into water from commercially available sock fabrics, Environmental Science and Technology 42 (2008) 4133–4139.
[24] J.-M. Chappé, N. Martin, J. Lintymer, F. Stahl, G. Terwagne, J. Takadoum, Titanium oxynitride thin films sputter deposited by the reactive gas pulsing process, Applied Surface Science 253 (2007) 5312–5316.
[25] F. Magnus, O. Sveinsson, S. Olafson, J. Gudmundsson, Current–voltage characteristics of the reactive Ar/N_2 high power impulse magnetron sputtering discharge, Journal of Applied Physics 110 (2011) 083306.
[26] J. Probst, U. Gbureck, R. Thull, Binary nitride and oxynitride PVD coatings on titanium for biomedical applications, Surface and Coatings Technology 148 (2001) 226–233.
[27] L. Wan, J. Li, J. Feng, W. Sun, Z. Mao, Improved optical response and photocatalysis for N-doped titanium oxide films prepared by oxidation of TiN, Applied Surface Science 253 (2007) 4764–4767.
[28] S. Lee, E. Yamasue, H. Okumura, K. Ishihara, Effect of oxygen and nitrogen concentration of nitrogen doped TiOx film as photocatalyst prepared by reactive sputtering, Applied Catalysis A-General 371 (2009) 179–190.
[29] O. Baghriche, J. Kiwi, C. Pulgarin, R. Sanjinés, Antibacterial Ag–ZrN surfaces promoted by Zr and deposited by reactive pulsed magnetron sputtering, Journal of Photochemistry and Photobiology A 229 (2012) 39–45.
[30] S. Rtimi, O. Baghriche, R. Sanjines, C. Pulgarin, M. Ben-Simon, J.-C. Lavanchy, A. Houas, J. Kiwi, Photocatalysis/catalysis by TiN/TiN-Ag surfaces efficient in bacterial inactivation under visible light, Applied Catalysis B 123–124 (2012) 306–315.
[31] S. Rtimi, O. Baghriche, C. Pulgarin, R. Sanjines, J. Kiwi, New evidence for sputtered TiN-surfaces able to inactivate bacteria undervisible light, RSC Advances 2 (2012) 8591–8595.
[32] J. Mathews, Epitaxial Growth Part B, IBM Thomas Watson Research Center, Academic Press, New York, 1975, pp. 382–436.
[33] D. Wagner, M. Riggs, E. Davis, G. Müllenberg (Eds.), Handbook of X-ray Photoelectron spectroscopy, Perkin-Elmer Corporation Physical Electronics Division, MN, 1979.
[34] D. Shirley, Corrections of electrostatic charged species in SP-spectroscopy, Physical Review B5 (1972) 4709–4716.
[35] B. Subramanian, C. Muraleedharan, R. Annanthakumar, M. Jayachandran, A comparative study of TiN, TiON and TiAlN as surface coatings for bioimplants, Surface and Coatings Technology 205 (2011) 5014–5020.
[36] C. Valentin, G. Pacchioni, A. Selloni, S. Livraghi, E. Giamello, Characterization of paramagnetic species in N-doped TiO_2 powders by EPR spectroscopy and DFT calculations, Journal of Physical Chemistry B 109 (2005) 11414–11419.
[37] Z. Lin, M. Orlov, C. Lambert, J. Payne, New insights into the origin of visible light photocatalytic activity of nitrogen-doped and oxygen-deficient anatase TiO_2, Journal of Physical Chemistry B 109 (2005) 20948–20952.
[38] R. Houk, B. Jacobs, F. Gabaly, N. Chang, D. Graham, S. House, M. Robertson, M. Allendorf, Silver cluster formation, dynamics, and chemistry in metal–organic frameworks, Nano Letters 9 (2009) 3413–3418.
[39] L. Gang, B. Anderson, L. Grondelle, R. Van Santen, Low temperature selective oxidation of ammonia to nitrogen on silver-based catalysts, Applied Catalysis B 40 (2002) 101–109.
[40] M. Kim, D. Stucky, Synthesis of highly ordered mesoporous silica materials using sodium silicate and amphiphilic block copolymers, Chemical Communications (2000) 1159–1160.
[41] V. Nadtochenko, A. Rincon, S. Stanka, J. Kiwi, Dynamics of *E. coli* photokilling due to cell wall lysis during TiO_2 photocatalysis, Journal of Photochemistry and Photobiology A 169 (2005) 131–137.
[42] R. Bacsa, J. Kiwi, J. Ohno, P. Albers, V. Nadtochenko, Preparation, testing and characterization of doped TiO_2 able to transform biomolecules under visible light irradiation by peroxidation/oxidation, Journal of Physical Chemistry B 109 (2005) 5994–6003.
[43] L. Heefner, Transport of H^+, K^+, N^+ and Ca^{2+} in Spretococcus, Molecular and Cellular Biochemistry 44 (1982) 81–89.
[44] Z. Lu, L. Zhou, Z. Zhang, W. Shi, Z. Xie, D. Pang, P. Shen, Cell damage induced by photocatalysis of TiO_2 thin films, Langmuir 19 (2003) 8765–8768.
[45] C. Huang, D. Maness, D. Blake, E. Wolfrum, E. Smolinski, W. Jacoby, Bactericide mode of TiO_2 photocatalysis, Journal of Photochemistry and Photobiology A 130 (2000) 163–170.
[46] P. Wu, R. Xie, K. Imlay, J. Shang, Visible light induced bactericidal activity of TiO_2 codoped with nitrogen and silver, Environmental Science and Technology 44 (2010) 6992–6997.

[47] P. Wu, R. Xie, J. Imlay, J. Shang, Visible light induced photocatalytic inactivation of bacteria by composite photocatalysts of PdO and N-doped TiO_2, Applied Catalysis 88 (2009) 481–576.
[48] Y. Jechandran, Sa. Naryandass, D. Mangalaraj, C. Bao, The effect of surface composition of titanium films on bacterial adhesion, Biomedical Materials 1 (2006) 1–5.
[49] Z. Aiken, G. Hyett, Ch. Dunnhill, M. Wilson, J. Pratten, P.I. Parkin, Antimicrobial activity in thin films of pseudobrookite-structured titanium oxynitride under UV-irradiation observed for *Esherichia coli*, Chemical Vapor Deposition 16 (2010) 19–22.
[50] G. Biedermann, G. Sillèn, Studies of the hydrolysis of metal-ions. Part 30. A critical survey of solubility equilibria of Ag_2O, Acta Chemica Scandinavica 14 (1969) 14–0717.
[51] Y. Ida, T. Watase, M. Shinagawa, M. Watabanbe, M. Chigane, M. Inaba, A. Tasaka, M. Izaki, Direct electrodeposition of 1.46 eV band-gap silver (I) oxide semiconductor films by electrogenerated acid, Chemistry of Materials 20 (2008) 1254–1256.
[52] A. Varkey, Some optical properties of silver peroxide (AgO) and silver oxide (Ag_2O) films produced by chemical-bath deposition, Solar Energy Materials and Solar Cells 29 (1993) 253–259.
[53] J. Yuand, J. Ran, Some optical properties of silver peroxide (AgO) and silver oxide (Ag_2O) films produced by chemical-bath deposition, Energy & Environmental Science 4 (2011) 1364–1371.
[54] H. Irie, S. Miura, K. Kamiya, K. Hashimoto, Efficient visible light-sensitive photocatalysts: grafting Cu(II) ions onto TiO_2 and WO_3 photocatalysts, Chemical Physics Letters 457 (2008) 202–205.